

# Analysis of Controlled Coherence Conversion in a Double Rephasing Scheme of Photon Echoes for Quantum Memories

Rahmatullah<sup>1,2</sup> and B. S. Ham<sup>1\*</sup>

<sup>1</sup>Center for Photon Information Processing, and School of Electrical Engineering and Computer Science, Gwangju Institute of Science and Technology, Gwangju, Republic of Korea and

<sup>2</sup>Quantum Optics Lab., Department of Physics, COMSATS Institute of Information Technology, Islamabad, Pakistan  
(Dated: December 14, 2016)

A controlled double rephasing (CDR) photon echo is analyzed for inversion-free photon echoes using controlled coherence conversion (CCC), where an optical Rabi flopping between an excited and an auxiliary ground states is used for atom phase control for emissive photon echoes. Unlike the rephasing mechanism in photon echoes, the CCC induces coherence inversion to the intrinsic absorptive echoes in a double rephasing scheme. Thus, the CDR echo protocol can be vastly applied for modified photon-echo quantum memories.

PACS numbers: 42.50.-p, 32.80 Qk, 42.50 Ct

## I. INTRODUCTION

Conventional photon echoes have been intensively studied for quantum memory applications over the last fifteen years since the first introduction of modification protocols of controlled reversible inhomogeneous broadening [1, 2], where the photon echo is a time-reversible macroscopic coherence burst induced by an optical  $\pi$  pulse [3]. Due to the inherent population inversion in photon echoes resulting in quantum noises as well as the violation of no cloning theorem [4], photon echo itself cannot be directly applied to quantum memories. Compared with single atom-based quantum memory protocols utilizing nuclear spins, e.g., recently demonstrated Si-based ultralong storage [5], the photon echoes in rare-earth doped solids have benefits of multimode, ultrafast, and ultrahigh absorption [6]. To overcome the inherent population inversion in photon echoes, atomic frequency comb (AFC) [7, 8], gradient echoes [9, 10], and controlled double rephasing (CDR) echoes [11, 12] are presented for quantum memory applications. Because ultralong quantum memory is an essential component of long-distance quantum communications based on quantum repeaters [13, 14], a storage time extension has also been a critical issue [15–18]. As experimentally demonstrated by using dynamic decoupling (DD) [14] and optical locking via controlled coherence conversion (CCC) [19], the optical storage time can be extended up to spin population decay time. However, in applications to quantum computers, DD-based quantum memories have limitations on frequent optical access for gate operations during storage, whereas CCC-based ones enjoy unlimited free access.

The CCC between optical and auxiliary spin states in ref. [11] has been proposed to convert the absorptive echo into an emissive echo in a double rephasing photon echo scheme. The double rephasing photon echo scheme inherently gives the benefit of no population inversion.

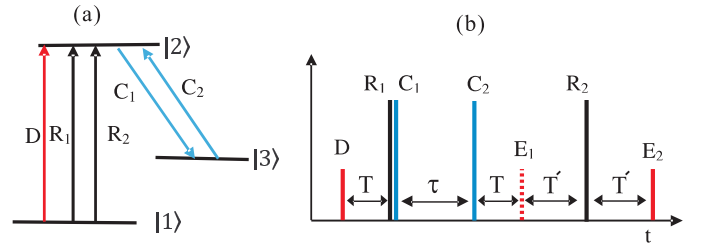


FIG. 1: (Color online) (a) Schematic of controlled double rephasing echoes. (b) Pulse sequence for (a).

Because rephasing itself in photon echoes results in a time reversal process owing to a  $\pi$  phase shift in collective atom coherence, the doubly rephased echo is absorptive due to a  $2\pi$  phase shift (no change) in coherence. Although silent echoes in a doubly rephased echo scheme have been successfully demonstrated [20–22], the echo cannot be radiated from the medium due to its absorptive coherence [20, 22]. Moreover, there is no way to solve this absorptive echo problem in a two-level system, at least not yet. Thus, conventional photon echoes have been deployed in a three-level system to control the collective atom phase for CDR echoes [12]. The CCC has already been discussed in a conventional two-pulse photon echo scheme theoretically [23] and experimentally [24]. Here, we present the physics of CCC in a double rephasing scheme of photon echoes with controlled Rabi flopping in a three-level system. Compared with full numerical analysis in previous discussions [11, 12, 16, 17, 23], we present full analytic solutions in this article.

## II. THEORY AND DISCUSSION

Figure 1 is a schematic diagram of the present CDR echoes, where the control pulse set of  $C_1$  and  $C_2$  is added for CCC in a three-level system as shown in Fig. 1(a). The data (D), first rephasing ( $R_1$ ) and second rephasing ( $R_2$ ) pulses satisfy a double rephasing photon echo

\*Electronic address: bham@gist.ac.kr

scheme, where they are resonant between states  $|1\rangle$  and  $|2\rangle$ . The pulse sequence of CDR is shown in Fig. 1(b), where the control pulse set  $C_1$  and  $C_2$  is resonant between states  $|2\rangle$  and  $|3\rangle$ . The time delay  $\tau$  between  $C_1$  and  $C_2$  is used for storage time extension [24, 25] limited by the spin dephasing  $(T_2^{\text{spin}})^*$ . In an optical locking scheme applied to three-pulse photon echoes [17], the storage time extends up to spin population decay time [19]. To satisfy general conditions of CDR as well as photon echoes, each pulse area of  $R_1$ ,  $R_2$ ,  $C_1$ , and  $C_2$  is set to be  $\pi$ . The pulse area of  $D$  is set to small at  $0.1\pi$ . The pulse area is defined by  $\varphi_i = \int \Omega_i dt$ , and  $\Omega_i (i = D, R_1, R_2, C_1 \text{ or } C_2)$  is the Rabi frequency of the pulse. The interaction picture Hamiltonian in the dipole and rotating-wave approximation of the proposed system can be written as:

$$H = -\hbar/2 \begin{bmatrix} 0 & \Omega_j & 0 \\ \Omega_j & 0 & \Omega_k \\ 0 & \Omega_k & 0 \end{bmatrix}, \quad (1)$$

where,  $\Omega_j (j = D, R_1 \text{ or } R_2)$  is the Rabi frequency of  $D$ ,  $R_1$  and  $R_2$ , and  $\Omega_k (k = C_1 \text{ or } C_2)$  is the Rabi frequency of  $C_1$  and  $C_2$ . We calculate the rate equations for the density matrix elements using Von Neumann equation:

$$\dot{\rho} = -\frac{i}{\hbar} [H, \rho] - \frac{1}{2} \{\Gamma, \rho\}. \quad (2)$$

Therefore, the corresponding rate equations are calculated as:

$$\dot{\rho}_{11} = -i \left[ \frac{\Omega_j}{2} (\rho_{12} - \rho_{21}) \right], \quad (3a)$$

$$\dot{\rho}_{22} = -i \left[ \frac{\Omega_j}{2} (\rho_{21} - \rho_{12}) + \frac{\Omega_k}{2} (\rho_{23} - \rho_{32}) \right], \quad (3b)$$

$$\dot{\rho}_{33} = -i \left[ \frac{\Omega_k}{2} (\rho_{32} - \rho_{23}) \right], \quad (3c)$$

$$\dot{\rho}_{12} = -i \left[ \frac{\Omega_j}{2} (\rho_{11} - \rho_{22}) + \frac{\Omega_k}{2} \rho_{13} \right], \quad (3d)$$

$$\dot{\rho}_{13} = -i \left[ \frac{\Omega_k}{2} \rho_{12} - \frac{\Omega_j}{2} \rho_{23} \right], \quad (3e)$$

$$\dot{\rho}_{23} = -i \left[ \frac{\Omega_k}{2} (\rho_{22} - \rho_{33}) - \frac{\Omega_j}{2} \rho_{13} \right], \quad (3f)$$

where, all decay rates are set to zero for simplicity. We consider two cases to present our analysis: (A) Double rephasing photon echoes and (B) CDR echoes.

### A. Double rephasing photon echoes

In this section, we study conventional two-pulse photon echoes in a double rephasing scheme, where the corresponding pulse sequence ( $D$ ,  $R_1$ , and  $R_2$ ) is without the CCC pulse set of  $C_1$  and  $C_2$  in Fig. 1(b). We follow the density matrix approach and derive the expressions for coherence and population for each pulse.

#### 1. D-pulse

The initial conditions before the application of the D-pulse are  $\rho_{11}(0) = 1$  and  $\rho_{22}(0) = \rho_{12}(0) = 0$ . We set  $\Omega_j = \Omega_D$  and  $\Omega_k = 0$  in equation (3) and the solutions of the density matrix elements for D-pulse are

$$\rho_{11} = \cos^2 \left( \frac{\varphi_D}{2} \right), \quad (4a)$$

$$\rho_{22} = \sin^2 \left( \frac{\varphi_D}{2} \right), \quad (4b)$$

$$\rho_{12} = -\frac{i}{2} \sin(\varphi_D), \quad (4c)$$

where  $\varphi_D$  is the area of the D-pulse. The detailed calculations for the derivation of equation (4) are given in Appendix B1. For maximum coherence the area of the D-pulse is set to be  $\pi/2$ , i.e.,  $\text{Im}[\rho_{12}] = -1/2$ . The negative sign denotes the absorption of the D-pulse. For a weak D-pulse  $\varphi_D \ll 1$ ,  $\rho_{11} \approx 1$ , the atomic population still remains in the ground state  $|1\rangle$ . In our analysis, we use a weak D-pulse of area  $0.1\pi$ .

#### 2. R<sub>1</sub>-pulse

The coherence created by the D-pulse starts to dephase until the rephasing pulse ( $R_1$ -pulse) is applied. We use equation (4) as initial condition and  $\Omega_j = \Omega_{R_1}$  in equation (3), and the solution of the rate equations for  $R_1$ -pulse is as followings:

$$\rho_{11} = \cos^2 \left( \frac{\varphi_D + \varphi_{R_1}}{2} \right), \quad (5a)$$

$$\rho_{22} = \sin^2 \left( \frac{\varphi_D + \varphi_{R_1}}{2} \right), \quad (5b)$$

$$\rho_{12} = -\frac{i}{2} \sin(\varphi_D + \varphi_{R_1}), \quad (5c)$$

where,  $\varphi_{R_1}$  is the  $R_1$ -pulse area. The rephasing  $\pi$  pulse swaps the coherence  $\rho_{12}$  initiated by the D-pulse of area  $0.1\pi$ , i.e., from  $-0.15$  to  $0.15$ , as shown in Fig. 2 (a):  $[\rho_{12}] \xrightarrow{R_1} [\rho_{12}]^*$  (see also Appendix A, where we use maximum coherence excitation by  $D$  of area  $\pi/2$ ). The  $\pi$  rephasing pulse swaps the population between ground and excited states as shown in Fig. 2 (b). The echo will be emitted from the excited state and thus the optical  $\pi$  pulse induces population inversion, and spontaneous emission noise becomes an issue for quantum memory applications. To overcome this limitation, a double rephasing concept is used [20–22]. For the double rephasing, another  $\pi$  pulse is applied to bring the atoms back to the ground state and a secondary echo is formed. As the secondary echo is radiated from the ground state, the spontaneous emission noise is suppressed. To fully restore the second echo as a copy of  $D$ , the first echo must be killed (erased or silenced) [20–22].

We derive the coherence and population rate equations for  $R_2$ -pulse by replacing  $\Omega_j$  with  $\Omega_{R_2}$  and setting

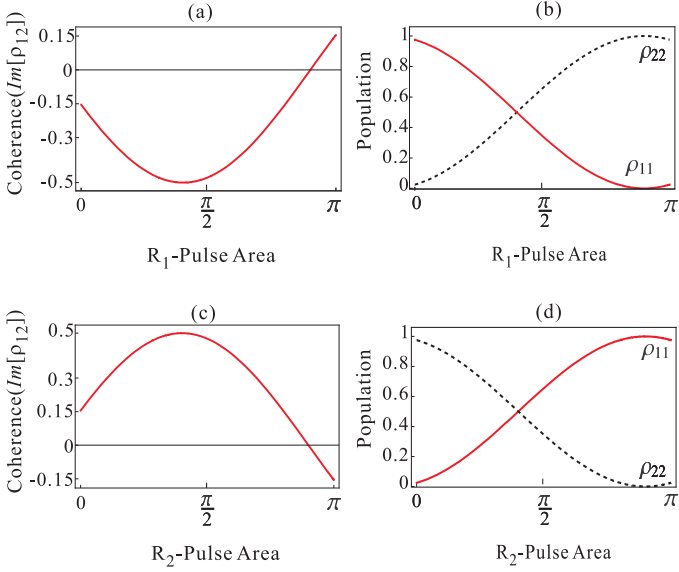


FIG. 2: (Color online) (a) Plot of  $Im[\rho_{12}]$  (equation 5c) versus  $R_1$ -pulse area  $\varphi_{R_1}$  with area of D-pulse  $\varphi_D = 0.1\pi$ . (b) Corresponding population evolution (red)  $\rho_{11}$  (equation 5a) and (dotted)  $\rho_{22}$  (equation 5b). (c) Plot of  $Im[\rho_{12}]$  (equation 6c) versus  $R_2$ -pulse area  $\varphi_{R_2}$ . The area of D-pulse is  $\varphi_D = 0.1\pi$  and  $R_1$  is  $\varphi_{R_1} = \pi$ . (d) Corresponding population evolution (red)  $\rho_{11}$  (equation 6a) and (dotted)  $\rho_{22}$  (equation 6b).

$\Omega_k = 0$  in equation (3). We use equation (5) as an initial condition and calculate the expressions for coherence and populations as:

$$\rho_{11} = \cos^2 \left( \frac{\varphi_D + \varphi_{R_1} + \varphi_{R_2}}{2} \right), \quad (6a)$$

$$\rho_{22} = \sin^2 \left( \frac{\varphi_D + \varphi_{R_1} + \varphi_{R_2}}{2} \right), \quad (6b)$$

$$\rho_{12} = -\frac{i}{2} \sin(\varphi_D + \varphi_{R_1} + \varphi_{R_2}). \quad (6c)$$

In Fig. 2(c) and 2(d), we plot the coherence and populations for  $\varphi_D = 0.1\pi$  and  $\varphi_{R_1} = \pi$ . The  $R_2$ -pulse inverts the coherence from 0.15 to -0.15. The negative sign shows the absorption of the coherence so the secondary echo is absorptive [11, 12]. Our aim is here, to get the inversion-free emissive echo. In the following section, we describe the role of  $C_1$  and  $C_2$  for CCC in detail.

## B. CDR echoes

For this section on CDR echoes, we add two control pulse set of  $C_1$  and  $C_2$  right after  $R_1$  as shown in Fig. 1(b). The control pulse position can also be inserted after  $R_1$  [11, 12].

### 1. $C_1$ -pulse

The control pulse  $C_1$  is applied to the  $|2\rangle \leftrightarrow |3\rangle$  transition. The  $C_1$ -pulse transfers population from state  $|2\rangle$  to an auxiliary spin state  $|3\rangle$ . The coherence and population equations for  $C_1$  can be obtained by using (5) as an initial condition. The time-dependent solution of density matrix equations (3) for  $C_1$  are calculated as:

$$\rho_{11} = \cos^2 \left( \frac{\varphi_D + \varphi_{R_1}}{2} \right), \quad (7a)$$

$$\rho_{22} = \cos^2 \left( \frac{\varphi_{C_1}}{2} \right) \sin^2 \left( \frac{\varphi_D + \varphi_{R_1}}{2} \right), \quad (7b)$$

$$\rho_{33} = \sin^2 \left( \frac{\varphi_{C_1}}{2} \right) \sin^2 \left( \frac{\varphi_D + \varphi_{R_1}}{2} \right), \quad (7c)$$

$$\rho_{12} = -\frac{i}{2} \cos \left( \frac{\varphi_{C_1}}{2} \right) \sin(\varphi_D + \varphi_{R_1}), \quad (7d)$$

$$\rho_{13} = -\frac{1}{2} \sin \left( \frac{\varphi_{C_1}}{2} \right) \sin(\varphi_D + \varphi_{R_1}), \quad (7e)$$

$$\rho_{23} = -\frac{i}{2} \sin(\varphi_{C_1}) \sin^2 \left( \frac{\varphi_D + \varphi_{R_1}}{2} \right). \quad (7f)$$

The detailed derivation of above equations appears in Appendix B 2. The optical coherence  $\rho_{12}$  in (7d) of  $C_1$ -pulse is equal to  $\cos(\varphi_{C_1}/2)$  times the coherence generated by  $R_1$ -pulse in (5c), which is equal to  $0.15i$  for  $0.1\pi$  of D-pulse and  $\pi$  of R-pulse. So we can write the coherence excited by the  $C_1$ -pulse for a fixed  $0.1\pi$  D-pulse and  $\pi$  R-pulse as  $Im[\rho_{12}] = 0.15 \cos(\varphi_{C_1}/2)$ . Similarly the spin coherence  $\rho_{13}$  in (7e) can be written as  $\rho_{13} = 0.15 \sin(\varphi_{C_1}/2)$ . In the absence of the  $C_1$ -pulse, i.e.,  $\varphi_{C_1} = 0$ ,  $Im[\rho_{12}] = 0.15$  and  $\rho_{13} = 0$ . The  $C_1$ -pulse of area  $\pi$  transfers the optical coherence excited by the  $R_1$  to the spin coherence, i.e.,  $Im[\rho_{12}] = 0$  and  $Re[\rho_{13}] = 0.15$  as shown in Fig. 3(a). Thus  $C_1$  locks the coherence evolution until  $C_2$  is applied if there is no spin dephasing. The  $C_1$ -pulse also shifts the population from the excited state  $|2\rangle$  to the auxiliary spin state  $|3\rangle$ . The population in the ground state  $|1\rangle$  is not affected by the  $C_1$  and remains the same as shown Fig. 3(b).

### 2. $C_2$ -pulse

The function of  $C_2$ -pulse is to restore the optical population from the auxiliary state  $|3\rangle$  back to the excited state  $|2\rangle$ . Using equation (7) as initial conditions,  $\Omega_k = \Omega_{C_2}$ , and  $\Omega_j = 0$  in equation (3), the coherence and population expressions for  $C_2$ -pulse are calculated as:

$$\rho_{11} = \cos^2 \left( \frac{\varphi_D + \varphi_{R_1}}{2} \right), \quad (8a)$$

$$\rho_{22} = \cos^2 \left( \frac{\varphi_{C_2} + \varphi_{C_1}}{2} \right) \sin^2 \left( \frac{\varphi_D + \varphi_{R_1}}{2} \right), \quad (8b)$$

$$\rho_{33} = \sin^2 \left( \frac{\varphi_{C_2} + \varphi_{C_1}}{2} \right) \sin^2 \left( \frac{\varphi_D + \varphi_{R_1}}{2} \right), \quad (8c)$$

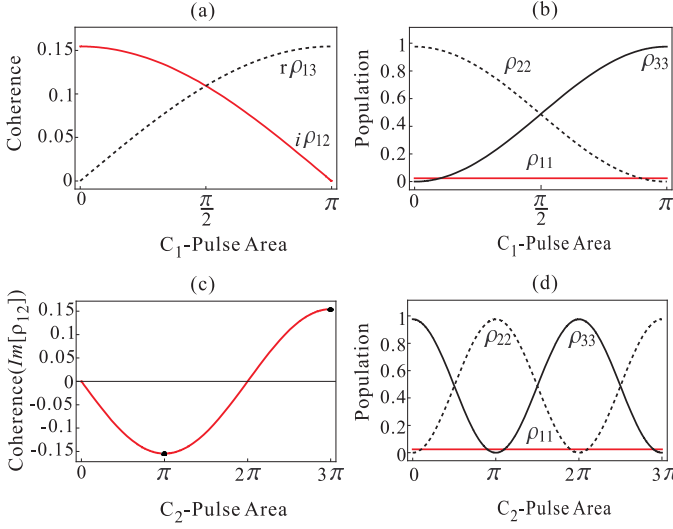


FIG. 3: (Color online) (a) Plot of  $Im[\rho_{12}]$  and  $Re[\rho_{13}]$  (equation 7d and 7e) versus  $C_1$ -pulse area  $\varphi_{C_1}$ . The area of D-pulse is  $\varphi_D = 0.1\pi$  and  $R_1$  is  $\varphi_{R_1} = \pi$ . (b) Corresponding population evolution (red)  $\rho_{11}$  (equation 7a), (dotted)  $\rho_{22}$  (equation 7b) and (black)  $\rho_{33}$  (equation 7c). (c) Plot of  $Im[\rho_{12}]$  (equation 8d) versus  $C_2$ -pulse area  $\varphi_{C_2}$ . The area of the other pulses are  $\varphi_D = 0.1\pi$ ,  $\varphi_{R_1} = \pi$  and  $\varphi_{C_1} = \pi$ . (d) Corresponding population evolution (red)  $\rho_{11}$  (equation 8a), (dotted)  $\rho_{22}$  (equation 8b) and (black)  $\rho_{33}$  (equation 8c) with  $\varphi_{C_1}$ .

$$\rho_{12} = -\frac{i}{2} \cos\left(\frac{\varphi_{C_2} + \varphi_{C_1}}{2}\right) \sin(\varphi_D + \varphi_{R_1}), \quad (8d)$$

$$\rho_{13} = -\frac{1}{2} \sin\left(\frac{\varphi_{C_2} + \varphi_{C_1}}{2}\right) \sin(\varphi_D + \varphi_{R_1}), \quad (8e)$$

$$\rho_{23} = -\frac{i}{2} \sin(\varphi_{C_2} + \varphi_{C_1}) \sin^2\left(\frac{\varphi_D + \varphi_{R_1}}{2}\right), \quad (8f)$$

The coherence (8d) is equal to the  $\cos\left(\frac{\varphi_{C_2} + \varphi_{C_1}}{2}\right)$  multiply by the coherence excited by  $R_1$ -pulse, (see equation 5c). In order to resume the coherence initiated by the  $R$ -pulse,  $(\varphi_{C_1} + \varphi_{C_2})$  must be equal to  $4n\pi$  ( $n = 1, 2, 3, \dots$ ). In other words the  $\pi$ - $\pi$  control pulse set induces coherence inversion [12]:  $\rho_{12} \xrightarrow{C_1 \& C_2} -\rho_{12}$ . In Fig. 3(c) and 3(d), we plot the coherence and population against the  $C_2$ -pulse area for  $\varphi_D = 0.1\pi$ ,  $\varphi_{R_1} = \pi$  and  $\varphi_{C_1} = \pi$ . Figure 3(c) shows that the coherence of  $R$ -pulse is resumed for  $C_2$ -pulse of area  $3\pi$ . The  $3\pi$   $C_2$  returns back the population to the excited state  $|2\rangle$  as shown in Figure 3(d). Unlike the  $(\pi$ - $\pi)$   $C_1$ - $C_2$  pulse sequence in controlled AFC [25], a  $\pi$ - $3\pi$  pulse sequence is necessary to the recovery of the coherence excited by the  $R_1$  [23]. The  $\pi$ - $\pi$  pulse sequence gives absorptive (negative) coherence, (see figure 3(c)), so no echo will be generated [11, 12]. In order to get emissive echo we combine the double rephasing technique with CCC by adding another rephasing pulse  $R_2$ : CDR. By the way ref. [21] uses controlled reversible inhomogeneous broadening [1], where reversed dc gradient fields results in emissive echo:  $\rho_{12} \rightarrow -\rho_{12}^*$ .

### 3. $R_2$ -pulse

The  $R_2$ -pulse returns back the population to the initial ground state  $|1\rangle$ . The pulse sequence for CDR is shown in figure 1(b). The solution of density matrix equations (3) for  $R_2$  by using equation (7) as initial condition is given as:

$$\rho_{11} = \frac{1}{16} \left[ \cos\left(\frac{\varphi_{C_2} + \varphi_{C_1} - \varphi_D - \varphi_{R_2} - \varphi_{R_1}}{2}\right) - \cos\left(\frac{\varphi_{C_2} + \varphi_{C_1} - \varphi_D + \varphi_{R_2} - \varphi_{R_1}}{2}\right) + 2\cos\left(\frac{\varphi_D - \varphi_{R_2} + \varphi_{R_1}}{2}\right) - \cos\left(\frac{\varphi_{C_2} + \varphi_{C_1} + \varphi_D - \varphi_{R_2} + \varphi_{R_1}}{2}\right) + \cos\left(\frac{\varphi_{C_2} + \varphi_{C_1} + \varphi_D + \varphi_{R_2} + \varphi_{R_1}}{2}\right) + 2\cos\left(\frac{\varphi_D + \varphi_{R_2} + \varphi_{R_1}}{2}\right) \right]^2, \quad (9a)$$

$$\rho_{22} = \frac{1}{16} \left[ \sin\left(\frac{\varphi_{C_2} + \varphi_{C_1} - \varphi_D - \varphi_{R_2} - \varphi_{R_1}}{2}\right) + \sin\left(\frac{\varphi_{C_2} + \varphi_{C_1} - \varphi_D + \varphi_{R_2} - \varphi_{R_1}}{2}\right) + 2\sin\left(\frac{\varphi_D - \varphi_{R_2} + \varphi_{R_1}}{2}\right) - \sin\left(\frac{\varphi_{C_2} + \varphi_{C_1} + \varphi_D - \varphi_{R_2} + \varphi_{R_1}}{2}\right) - \sin\left(\frac{\varphi_{C_2} + \varphi_{C_1} + \varphi_D + \varphi_{R_2} + \varphi_{R_1}}{2}\right) - 2\sin\left(\frac{\varphi_D + \varphi_{R_2} + \varphi_{R_1}}{2}\right) \right]^2, \quad (9b)$$

$$\rho_{33} = \sin^2\left(\frac{\varphi_{C_2} + \varphi_{C_1}}{2}\right) \sin^2\left(\frac{\varphi_D + \varphi_{R_1}}{2}\right), \quad (9c)$$

$$\rho_{12} = -\frac{i}{16} \left[ 2\sin(\varphi_{R_2}) + 2\sin(\varphi_{R_2}) \cos(\varphi_D + \varphi_{R_1}) \left(3 + \cos\left(\frac{\varphi_{C_2} + \varphi_{C_1}}{2}\right)\right) + \sin(\varphi_{C_2} + \varphi_{C_1} - \varphi_{R_2}) - \sin(\varphi_{C_2} + \varphi_{C_1} + \varphi_{R_2}) + 8\cos\left(\frac{\varphi_{C_2} + \varphi_{C_1}}{2}\right) \cos(\varphi_{R_2}) \sin(\varphi_D + \varphi_{R_1}) \right]. \quad (9d)$$

In a double rephasing scheme, we consider  $(\pi$ - $\pi)$   $C_1$  -  $C_2$  pulse sequence. In Fig. 4, we plot the evolution of the

coherence and populations as a function of  $\pi$   $R_2$ -pulse

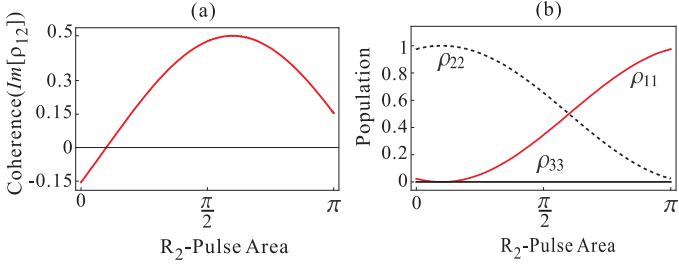


FIG. 4: (Color online) (a) Plot of  $Im[\rho_{12}]$  (equation 9d) versus  $R_2$ -pulse area  $\varphi_{R_2}$ . The area of the other pulses are  $\varphi_D = 0.1\pi$ ,  $\varphi_{R_1} = \pi$ ,  $\varphi_{C_1} = \pi$  and  $\varphi_{C_2} = \pi$ . (b) Corresponding population evolution (red)  $\rho_{11}$  (equation 9a), (dotted)  $\rho_{22}$  (equation 9b) and (black)  $\rho_{33}$  (equation 9c).

area for  $\varphi_D = 0.1\pi$ ,  $\varphi_{R_1} = \pi$ ,  $\varphi_{C_1} = \pi$  and  $\varphi_{C_2} = \pi$ . The initial coherence is inverted with population in the ground state, and spontaneous emission, noise-free photon echo  $E_2$  is ready due to the silent echo  $E_1$ .

### III. CONCLUSION

In conclusion, we analytically presented the CDR echo for a spontaneous emission, noise-free photon echo protocol by combining double rephasing method with CCC. The density matrix equations were solved for each pulse and coherence evolutions were demonstrated with analytic expressions. Our proposed scheme would solve the absorptive photon echo problem in a double rephasing scheme. The role of the control pulses was also investigated for coherence inversion with  $4n\pi$  ( $n = 1, 2, 3..$ ) pulse area.

#### Acknowledgment

This work was supported by the ICT R&D program of MSIP/IITP (1711028311: Reliable crypto-system standards and core technology development for secure quantum key distribution network), and GIST-Caltech program in 2016.

#### Appendix A: Coherence swapping using $\pi/2$ D-pulse

In this Appendix, we analyze the coherence swapping for reshaping and control pulses using  $\pi/2$  D-pulse. The D-pulse creates coherence between the  $|1\rangle \leftrightarrow |2\rangle$  transition ( $Im[\rho_{12}] = -0.5$ , using equation (4c) for  $D = \pi/2$ ). The negative sign depicts the absorption of the D-pulse. In Fig. 5, we show the retrieval of this initial coherence by using reshaping and control pulses. The first rephasing pulse  $R_1$  switches the coherence from absorption to emission as shown in Fig. 5(a). The rephasing  $\pi$   $R_1$ -pulse also transfers the population to the excited

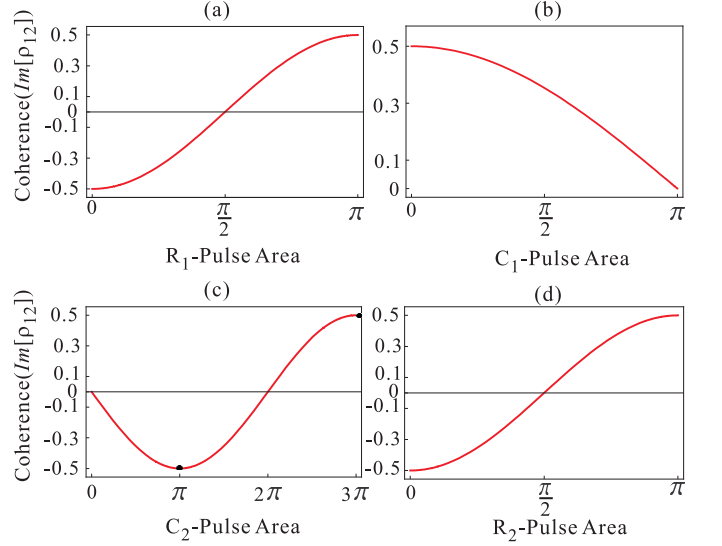


FIG. 5: (Color online) (a) Plot of  $Im[\rho_{12}]$  versus (a)  $R_1$ -pulse area  $\varphi_{R_1}$  (Eq. 5c), (b)  $C_1$ -pulse area  $\varphi_{C_1}$  (Eq. 7d), (c)  $C_2$ -pulse area  $\varphi_{C_2}$  (Eq. 8d) and (d)  $R_2$ -pulse area  $\varphi_{R_2}$  (Eq. 9d). The area of the D-pulse  $\varphi_D = \pi/2$ .

state, so the echo also should suffer from spontaneous emission noise.

To control coherence of atoms, we use two control pulses  $C_1$  and  $C_2$ . The  $C_1$ -pulse shifts the population from the excited state to an auxiliary spin state. Then coherence evolution is locked if there is no spin dephasing, i.e.,  $Im[\rho_{12}] = 0$  as shown in Fig. 5(b). In order to resume the coherence, we apply  $C_2$ -pulse which also brings the population back to the excited state. The coherence is absorptive (negative) for  $\pi$   $C_2$ -pulse and emissive (positive) for  $3\pi$   $C_2$ -pulse, (see the dots in Fig. 5(c)). In Fig. 5(d), we recover the same coherence as that by the D-pulse, by using second rephasing pulse  $R_2$  of area  $\pi$ . For this  $C_2$  is set  $\pi$ .

#### Appendix B: Solution of density matrix equations

The analytical expressions are obtained by solving the density matrix equations (3) for each pulse. In appendices B1 and B2, we derive the analytical solutions for populations and coherences for D and  $C_1$  pulses, respectively. The expressions for other pulses are calculated in the same line.

##### 1. (Analytical solution for D-pulse)

For the D-pulse, we set  $\Omega_j = \Omega_D$  and  $\Omega_k = 0$  in equation (3). The equations of motion for D-pulse are:

$$\dot{\rho}_{11} = -i\frac{\Omega_D}{2}(\rho_{12} - \rho_{21}), \quad (B1a)$$

$$\dot{\rho}_{22} = -i\frac{\Omega_D}{2}(\rho_{21} - \rho_{12}), \quad (\text{B1b})$$

$$\dot{\rho}_{12} = -i\frac{\Omega_D}{2}(\rho_{11} - \rho_{22}), \quad (\text{B1c})$$

$$\dot{\rho}_{21} = -i\frac{\Omega_D}{2}(\rho_{22} - \rho_{11}). \quad (\text{B1d})$$

Initially all population is in the ground state, i.e.,  $\rho_{11}(0) = 1$  and  $\rho_{22}(0) = \rho_{12}(0) = \rho_{21}(0) = 0$ . Equations (B1a)-(B1d) are first order coupled differential equations, and there are several methods to solve these equations. Here, we use Laplace transform with  $\rho_{11} + \rho_{22} = 1$ . The Laplace transform of equation (B1) yields:

$$s\mathcal{L}[\rho_{11}] = 1 - \frac{i\Omega_D}{2}(\mathcal{L}[\rho_{12}] - \mathcal{L}[\rho_{21}]), \quad (\text{B2a})$$

$$s\mathcal{L}[\rho_{12}] = -\frac{i\Omega_D}{2}\left(2\mathcal{L}[\rho_{11}] - \frac{1}{s}\right), \quad (\text{B2b})$$

$$s\mathcal{L}[\rho_{21}] = \frac{i\Omega_D}{2}\left(2\mathcal{L}[\rho_{11}] - \frac{1}{s}\right). \quad (\text{B2c})$$

The solutions of equation (B2) can be written as:

$$\mathcal{L}[\rho_{11}] = \frac{2s^2 + \Omega_D^2}{2s(s^2 + \Omega_D^2)}, \quad (\text{B3a})$$

$$\mathcal{L}[\rho_{12}] = \frac{-i\Omega_D}{s^2 + \Omega_D^2}, \quad (\text{B3b})$$

$$\mathcal{L}[\rho_{21}] = \frac{i\Omega_D}{s^2 + \Omega_D^2}. \quad (\text{B3c})$$

The final equations for population and coherence are obtained by taking the inverse Laplace transform of equation (B3):

$$\rho_{11} = \cos^2\left(\frac{\varphi_D}{2}\right), \quad (\text{B4a})$$

$$\rho_{22} = \sin^2\left(\frac{\varphi_D}{2}\right), \quad (\text{B4b})$$

$$\rho_{12} = -\frac{i}{2}\sin(\varphi_D), \quad (\text{B4c})$$

$$\rho_{21} = \frac{i}{2}\sin(\varphi_D). \quad (\text{B4d})$$

Similarly, we calculate the expressions for  $R_1$ -pulse by using equation (B4) as an initial condition.

## 2. (Analytical solution for $C_1$ -pulse)

The  $C_1$ -pulse is resonant for  $|2\rangle \leftrightarrow |3\rangle$  transition, and density matrix equations for  $C_1$  are obtained by replacing  $\Omega_k = \Omega_{C_1}$  and setting  $\Omega_j = 0$  in equation (3):

$$\dot{\rho}_{22} = -i\frac{\Omega_{C_1}}{2}(\rho_{23} - \rho_{32}), \quad (\text{B5a})$$

$$\dot{\rho}_{33} = -i\frac{\Omega_{C_1}}{2}(\rho_{32} - \rho_{23}), \quad (\text{B5b})$$

$$\dot{\rho}_{12} = -i\frac{\Omega_{C_1}}{2}\rho_{13}, \quad (\text{B5c})$$

$$\dot{\rho}_{13} = -i\frac{\Omega_{C_1}}{2}\rho_{12}, \quad (\text{B5d})$$

$$\dot{\rho}_{23} = -i\frac{\Omega_{C_1}}{2}(\rho_{22} - \rho_{33}). \quad (\text{B5e})$$

We set equation (5) as an initial condition, i.e.,

$$\rho_{11}(0) = \cos^2\left(\frac{\varphi_D + \varphi_{R_1}}{2}\right), \quad (\text{B6a})$$

$$\rho_{22}(0) = \sin^2\left(\frac{\varphi_D + \varphi_{R_1}}{2}\right), \quad (\text{B6b})$$

$$\rho_{12}(0) = -\frac{i}{2}\sin(\varphi_D + \varphi_{R_1}), \quad (\text{B6c})$$

$$\rho_{33}(0) = \rho_{13}(0) = \rho_{23}(0) = 0. \quad (\text{B6d})$$

The Laplace transform of the equation (B5) gives:

$$s\mathcal{L}[\rho_{22}] - \rho_{22}(0) = -i\frac{\Omega_{C_1}}{2}(\mathcal{L}[\rho_{23}] - \mathcal{L}[\rho_{32}]), \quad (\text{B7a})$$

$$s\mathcal{L}[\rho_{33}] - \rho_{33}(0) = -i\frac{\Omega_{C_1}}{2}(\mathcal{L}[\rho_{32}] - \mathcal{L}[\rho_{23}]), \quad (\text{B7b})$$

$$s\mathcal{L}[\rho_{12}] - \rho_{12}(0) = -i\frac{\Omega_{C_1}}{2}\mathcal{L}[\rho_{13}], \quad (\text{B7c})$$

$$s\mathcal{L}[\rho_{13}] - \rho_{13}(0) = -i\frac{\Omega_{C_1}}{2}\mathcal{L}[\rho_{12}], \quad (\text{B7d})$$

$$s\mathcal{L}[\rho_{23}] - \rho_{23}(0) = -i\frac{\Omega_{C_1}}{2}(\mathcal{L}[\rho_{22}] - \mathcal{L}[\rho_{33}]). \quad (\text{B7e})$$

The solutions of the equation (B7) by using equation (B6) can be written as:

$$\mathcal{L}[\rho_{22}] = \frac{(2s^2 + \Omega_{C_1}^2)}{2s(s^2 + \Omega_{C_1}^2)}\sin^2\left(\frac{\varphi_D + \varphi_{R_1}}{2}\right), \quad (\text{B8a})$$

$$\mathcal{L}[\rho_{33}] = \left(\frac{\Omega_{C_1}^2}{2s(s^2 + \Omega_{C_1}^2)}\right)\sin^2\left(\frac{\varphi_D + \varphi_{R_1}}{2}\right), \quad (\text{B8b})$$

$$\mathcal{L}[\rho_{12}] = -\frac{i}{2}\sin(\varphi_D + \varphi_{R_1})\left(\frac{4s}{4s^2 + \Omega_{C_1}^2}\right), \quad (\text{B8c})$$

$$\mathcal{L}[\rho_{13}] = -\frac{1}{2}\sin(\varphi_D + \varphi_{R_1})\left(\frac{2\Omega_{C_1}}{4s^2 + \Omega_{C_1}^2}\right), \quad (\text{B8d})$$

$$\mathcal{L}[\rho_{23}] = -\frac{i}{2}\sin^2\left(\frac{\varphi_D + \varphi_{R_1}}{2}\right)\left(\frac{\Omega_{C_1}}{s^2 + \Omega_{C_1}^2}\right). \quad (\text{B8e})$$

The inverse Laplace transform yields the final solution for  $C_1$ -pulse as given in equation (7). In the same way the analytical solutions of population and coherence for  $C_2$ -pulse are also obtained by using the final equation of  $C_1$  as an initial condition.

- 
- [1] S. A. Moiseev and S. Kröll, Phys. Rev. Lett. **87**, 173601 (2001).
  - [2] S. A. Moiseev, V. F. Tarasov, and B. S. Ham, J. Opt. B: Quantum Semiclassical Optics **5**, S497 (2003).
  - [3] N. A. Kurnit, I. D. Abella, and S. R. Hartmann, Phys. Rev. Lett. **13**, 567568 (1964).
  - [4] W. K. Wootters and W. H. Zurek, Nature **299**, 802-803 (1982).
  - [5] E. Togan *et al.*, Quantum entanglement between an optical photon and a solid-state spin qubits. Nature **466**, 730-734 (2010).
  - [6] R. M. Macfarlane and R. M. Shelby, *Coherent transient and holeburning spectroscopy of rare earth ions in solids*, in *Spectroscopy of solids containing rare earth ions*, Kaplyanskii, A. and Macfarlane, R. M., eds. (North-Holland, 1987).
  - [7] H. de Riedmatten *et al.*, Nature **456**, 773 (2008).
  - [8] W. Tittel *et al.*, Laser and Photon. Rev. **4**, 244-267 (2010).
  - [9] G. Hétet *et al.*, Phys. Rev. Lett. **100**, 023601 (2008).
  - [10] M. P. Hedges, J. J. Longdell, Y. Li, and M. J. Sellars, Nature **465**, 1052-1056 (2010).
  - [11] B. S. Ham, Atom phase controlled noise-free photon echoes, arXiv:1101.5480 (2011).
  - [12] B. S. Ham, Collective atom phase controls in photon echoes for quantum memory applications I: Population inversion removal, arXiv:1612.00115 (2016).
  - [13] L.-M. Duan, M. D. Lukin, J. I. Cirac, and P. Zoller, Nature **414**, 413-418 (2001).
  - [14] N. Sangouard, C. Simon, H. de Riedmatten, and N. Gisin, Rev. Mod. Phys. **83**, 33 (2011).
  - [15] J. J. Longdell, E. Fraval, M. J. Sellars, and N. B. Manson, Phys. Rev. Lett. **95**, 063601 (2005).
  - [16] B. S. Ham, Nature Photon. **3**, 518 (2009).
  - [17] B. S. Ham, Phys. Rev. A **85**, 031402(R) (2012); *ibid*, **94**, 049905 (2016).
  - [18] L. Langer *et al.*, Nature Photon. **8**, 851 (2014).
  - [19] B. S. Ham, New J. Phys. **14**, 013003 (2012).
  - [20] V. Damon *et al.*, New. J. Phys. **13**, 093031 (2011).
  - [21] McAuslan, D. L. *et al.* Phys. Rev. A **84**, 022309 (2011).
  - [22] A. Arcangeli, A. Ferrier, and Ph. Goldner, Phys. Rev. A **93**, 062303 (2016).
  - [23] B. S. Ham, Opt. Exp. **18**, 1704-1713 (2010).
  - [24] J. Hahn and B. S. Ham, New J. Phys. **13**, 093011 (2011).
  - [25] M. Afzelius *et al.* Phys. Rev. Lett. **104**, 040503 (2010).